DOI: 10.13009/EUCASS2019-379

Investigating the Aerodynamic Interference of Control Surfaces by Artificial Neural Networks

Fazil Selcuk Gomec Dr. Sukru Akif ERTURK** Osman AYCI***
**Aerodynamics Department, Turkish Aerospace*
Ankara 06980, Turkey
***Modelling Department, Turkish Aerospace*
Ankara 06980, Turkey

Abstract

In critical design phase of aircraft, the success of stability, control and performance computations are strongly dependent upon the reliability of plant models. The aerodynamic efforts stand on the center of these models. Almost every system is fed by the aerodynamic coefficients and they should be modelled as much as accurate. It requires the investigation of the interference effects between primary and secondary control surfaces. In this study, aerodynamic interference effects between horizontal tail-rudder, trailing edge flap-horizontal tail and trailing-leading edge flaps are computed. Artificial neural networks, super-impose, linear and cubic spline interpolations are employed and their results are compared.

1. Introduction

Aerodynamic database of an aircraft is composed of computational and experimental processes. Computational fluid dynamics (CFD), wind tunnel and flight tests are widely involved in database generations. Force and moment coefficients of the baseline configuration for the static and dynamic conditions, primary or secondary control surface deflections, speed brakes and landing gear configurations are represented in this database [1] [2] [3].

The created aerodynamic database are combined with the mass properties, engine database, and the atmospheric properties to build up the six degrees of freedom (6-DOF) model of the aircraft including the actuator, sensor and engine dynamics. The 6-DOF aircraft models are used for flight mechanics and performance analyses to determine the characteristics of the designed aircraft. These models are also employed as a plant by control engineers to design a control system and in the engineering or flight training simulators. Therefore, the model should represent the aircraft dynamics as much as accurate.

Neural Network (NN) based modeling is used for different aircraft applications. For instance, aerodynamic forces and moments were modeled with artificial neural networks including nonlinear unsteady post-stall aerodynamics cases [4]. In addition to aerodynamic model, metamodels were formed for propulsion and mass properties for the nonlinear 6-DOF aircraft model [5]. Furthermore, rotorcraft aeromechanics such as helicopter vibrations in real time were modeled to obtain high fidelity during piloted simulations [6]. The pilot's visual cues during landing were modeled using the information about the horizon, runway shape, and runway marker by neural network [7]. Another application was to model the fuel consumptions from the data given in the aircraft performance manual for different flight conditions such as climb, cruise and descent [8].

In the 6-DOF models, delta effects of the control surface deflections, landing gear, speed brake or the other effective components should be discriminated to represent the aerodynamic characteristics. Moreover, their interference effects in the aerodynamic database should be focused since significant changes can be observed with multiple control surface deflections, especially in maneuvering conditions [9]. For instance, the combination of the trailing edge flap and horizontal tail deflections affects each other independent from their single deflections. These effects must be reflected to the 6-DOF model for more accurate simulation results.

Levin investigated the interactions between a swept-wing and canard by a vortex lattice method. Significant effects were observed on the wing performance due to the leading edge separations of thin airfoils at subsonic flow regimes

DOI: 10.13009/EUCASS2019-379

[10]. Also, Elzebda et al. studied the canard and wing interactions and clearly isolated lift and drag values for both of them [11]. Moore and McInville proposed a semi empirical method for the wing and tail interferences of a missile at high angle of attack and Mach regimes [12]. As a different point of view, Kulfan has researched favorable aspect of aerodynamic interference effects like decreasing wave drag in supersonic flights [13]. Landman et al. conducted wind tunnel tests with trijet-blended wing body concept of Boeing. They investigated the control surface interactions with the help of design of experiment and response surface techniques [14].

In this study, computational fluid dynamics (CFD) and wind tunnel based aerodynamic database of HURJET that is a jet trainer aircraft is investigated in the aspect of control surface interferences. It should be noted that subsonic and transonic flight conditions are included in the database. Interferences between horizontal tail-rudder, trailing edge flap-horizontal tail and leading edge flap-trailing edge flaps are evaluated with three different approaches. In the first and second approaches, linear and cubic-spline techniques are focused for these effects. In the third one, an optimized neural network code, which is called NNGA, is utilized to discriminate the interferences and single deflection effects. NNGA is an artificial neural network code which is optimized by genetic algorithm [15]. All this data compared with the simple super-impose technique which does not include interference effects. Since the wind tunnel tests are in the limited number, results of them are used to point out which coefficients will be considered in the aspect of interference.

2. Aircraft Geometry

In the interference studies, the preliminary design of HURJET, is evaluated. It is a part of jet trainer program. The maximum speed and maximum altitude targets are selected as 1.2 Mach and 45,000ft. Aileron, rudder, horizontal tail and flaps are the primary and secondary control systems of this aircraft. Flaps have two settings for the landing and takeoff configurations. Moreover, aileron and flaps can be replaced with a flaperon in future designs. The flap interferences should be evaluated with noting this update. The aircraft with the relevant surface mesh is shown in Figure 1. Since the landing gear interference is not in the scope of this study, the geometry of nose and main landing gears are not shown in this figure.

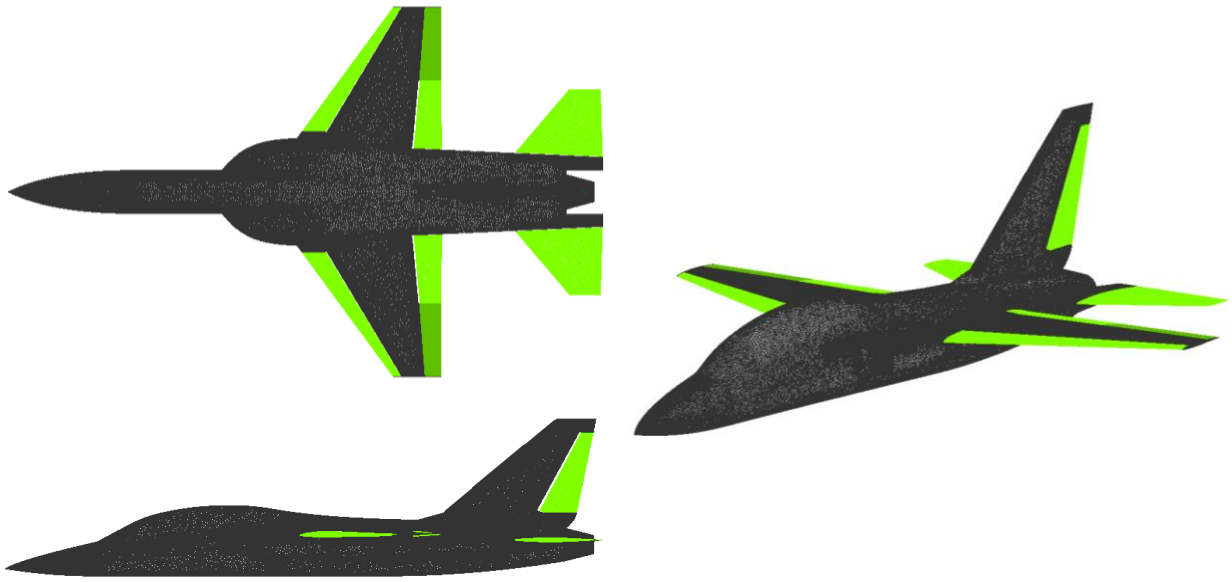

Figure 1: Top, side and isometric views of HURJET

3. Wind Tunnel Evaluations

The interference effects were conducted in the wind tunnel tests of the Hurjet. These tests are done at the limited number of analyses. The results of these tests guide this study in the aspects of which effects should be focused in the CFD simulations. Since the test data are on the wind tunnel scale, the results are not compared with the CFD simulations.

DOI: 10.13009/EUCASS2019-379

Two different cases are given in the figures. The *SuperImpose* case is the sum of single deflection effects on the baseline geometry. The *WindTunnel* case is the results of the geometry those all related surfaces are deflected during the tests. The results of both cases are the outputs of the wind tunnel.

Figure 2 shows the interference effects between the trailing edge flap and horizontal tail deflections at the flow velocity of 0.3 Mach. It should be noted that both flaps are deflected as 30° while only the left-horizontal tail deflected as 10°. As seen from this figure, lift and drag coefficients change slightly while the pitch moment differs significantly with interference effects. Also, the side force and yaw coefficients are almost identical for both cases. Although the roll moment coefficient is moderately different, it is originated from testing only left horizontal tail. In other words, the changes in the roll moment coefficient can also be ignored. Therefore, the interference effects between the horizontal tail and the trailing edge flap should be evaluated only in angle of attack variations of lift force, drag force and pitch moment.

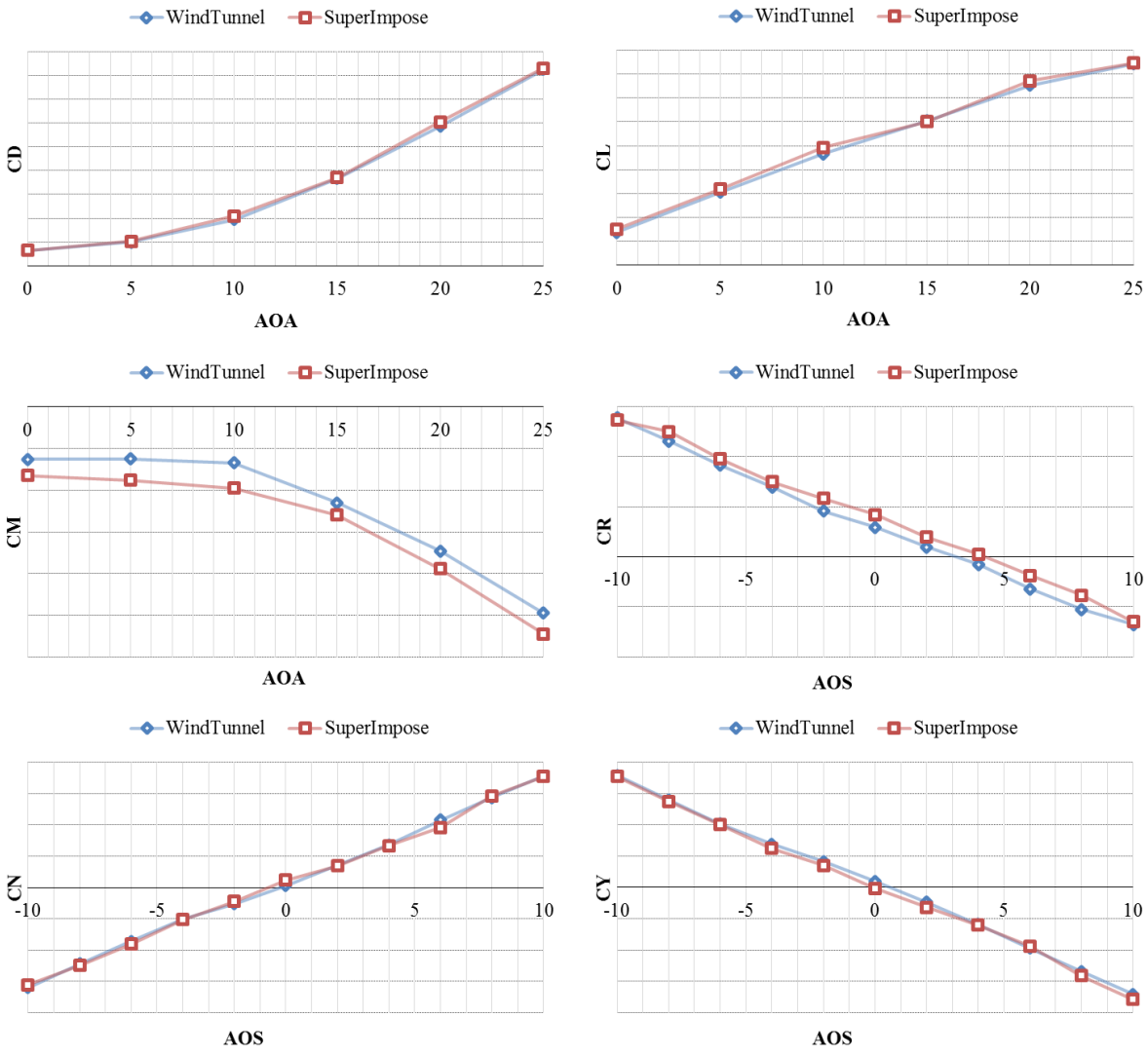

Figure 2: Horizontal tail(*+10°*) and trailing edge flap(*+30°*) interference comparison in a wind tunnel, 0.3 Mach

Influence of the trailing edge flap on the rudder deflections are given in Figure 3. In this figure, the rudder is deflected as 20° while the flap position is 30°.

DOI: 10.13009/EUCASS2019-379

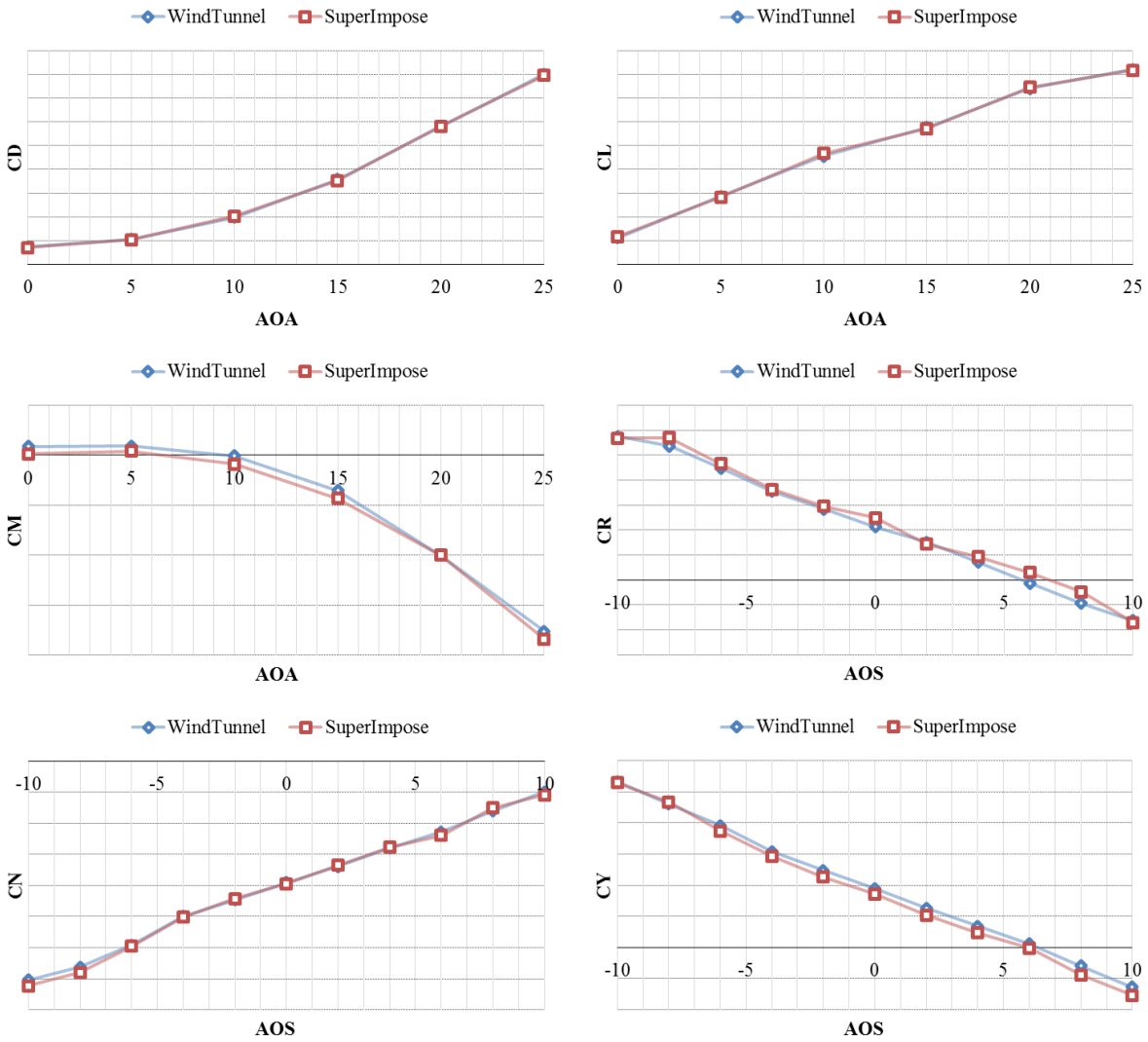

Figure 3: Rudder(*+20°*) and trailing edge flap(*+30°*) interference comparison in a wind tunnel, 0.3 Mach

As seen from Figure 3, there is no significant influence on the lift, drag and yaw moment coefficients. Contrarily, there are relatively small shifts in pitch moment and side force coefficients as compared to rudder and horizontal tail interference. Also, small number of fluctuations observed in the roll moment coefficient especially at higher sideslip angles. Nevertheless, these differences are not valuable to compare neural network analyses with linear and cubic splines. Rudder and trailing edge flap interference effects are not evaluated in the scope of this study. Nevertheless, it should be noted that flaperons have impacts on the rudder outputs especially in asymmetric deflections.

In Figure 4 and Figure 5, rudder and horizontal tail interference effects are given at 0.6 Mach. Two different deflections of horizontal tail and only one deflection of the rudder are shown in these figures.

The interference between the horizontal tail deflection and rudder interference are almost insignificant in lift force, drag force and pitch moment characteristics. However, the effects of interference in lateral and directional characteristics are certain and can be clearly observed in these figures. Therefore, the interference between the rudder and horizontal tail should be computed with respect to the sideslip angle variations.

DOI: 10.13009/EUCASS2019-379

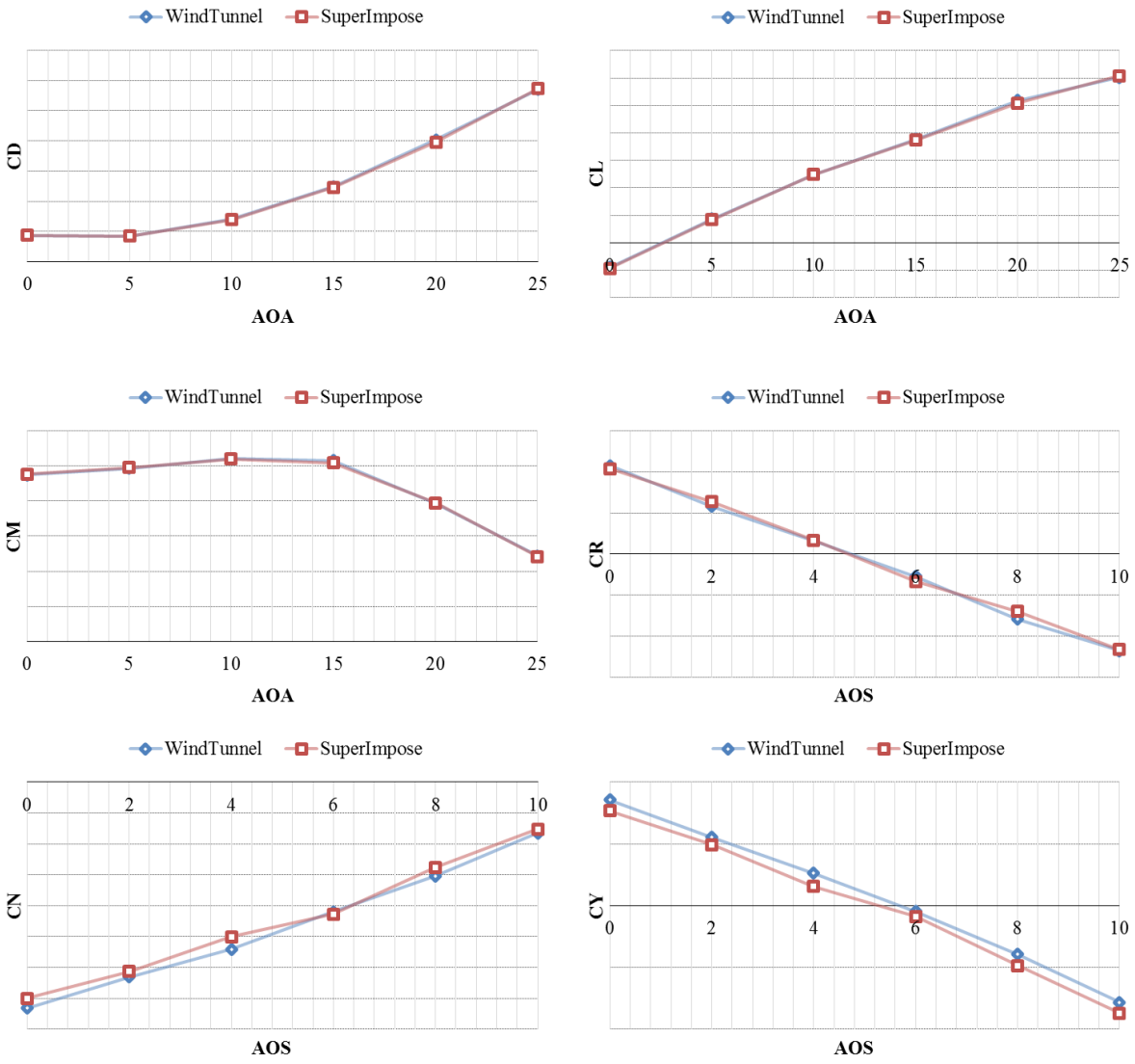

Figure 4: Horizontal tail(*-20°*) and rudder(*+20°*) interference comparison in a wind tunnel, 0.6 Mach

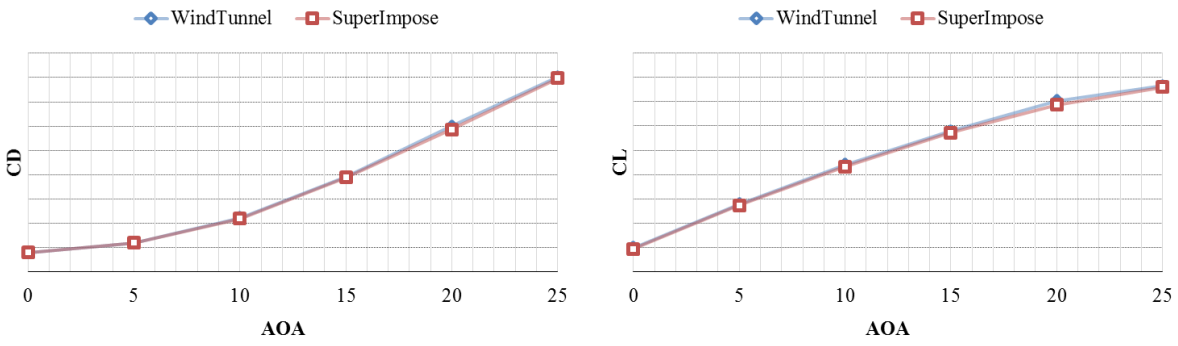

Figure 5: Horizontal tail(*+20°*) and rudder(*+20°*) interference comparison in a wind tunnel, 0.6 Mach

DOI: 10.13009/EUCASS2019-379

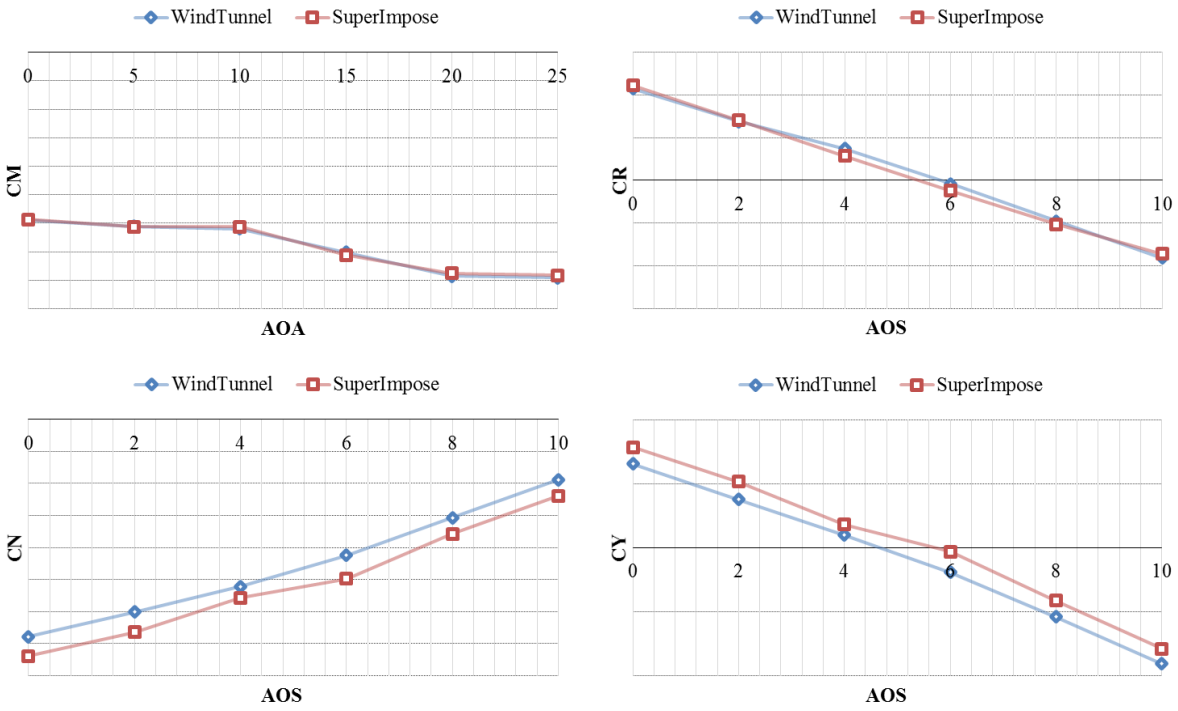

Figure 5 (cont): Horizontal tail(*+20°*) and rudder(*20°*) interference comparison in a wind tunnel, 0.6 Mach

Although the interferences in leading and trailing edge flaps are not tested in the wind tunnel campaign for the subsonic flow fields, these interferences should be analyzed with CFD simulations. In summary, interference effects between rudder-horizontal tail, trailing edge flap-horizontal tail and leading-trailing edge flaps are studied in this study. CFD analyses are employed to reveal these effects elaborately.

4. Plant Model and Flight Conditions

To obtain the effective breakpoints for the interference computations, trim points should be determined. A plant model is required to compute these points. HURJET plant model representation is presented as block diagrams in Figure 6. In this nonlinear model, atmospheric model, mass properties model, engine model, landing gear model, aerodynamic model and the 6-DOF equations of motions are integrated and built in MATLAB®/Simulink environment. In the plant model, forces and moments from the engine model, the landing gear model, the mass properties model and the aerodynamic model are the inputs of the equations of motions to represent the 6-DOF dynamic model.

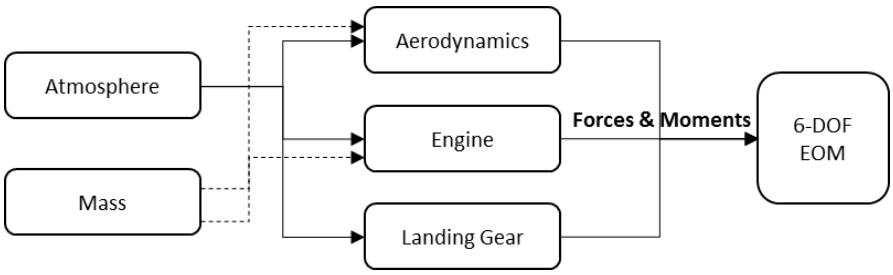

Figure 6: HURJET Plant Model Block Diagram

The maneuvers such as cruise, climb, descent, pull up, coordinated turn, steady heading sideslip are defined for the specified steady-state flight conditions in terms of the inputs and the states required after trimming and linearizing the 6-DOF nonlinear model.

In the aerodynamic model, linear super-impose technique is used to calculate aerodynamic forces and moments coefficients of the aircraft. In the CFD analyses, single control surface deflections are considered to reduce the

DOI: 10.13009/EUCASS2019-379

computational time for generating aerodynamic model. Hence, the aerodynamic coefficients are the summation of the single delta effects of each control surface and the clean configuration with the super-impose technique. The clean configuration means that the aircraft does not have any deflections, at a specified flight condition. In this method, the aerodynamic interference effects of combined control surface deflections are not taken into account.

To analyze the aerodynamic interference effects, trim conditions at different flight phases are examined by using the plant model. These trim conditions are used to determine the convenient aerodynamic database breakpoints to reduce the CFD analyses runs. As an example study, trim conditions for the high sideslip angles are shown in Figure 7. The rudder and horizontal tail deflections at different altitudes are provided in this figure since the maximum rudder deflections are required at this flight phase. Based on these analyses, rudder and horizontal tail deflection breakpoints of the aerodynamic database are selected between [0, 25] degrees for rudder, and [-15, 5] degrees for horizontal tail as tabulated in Table 1. The rest of the breakpoints shown in Tables 2-3 are determined with the same approach.

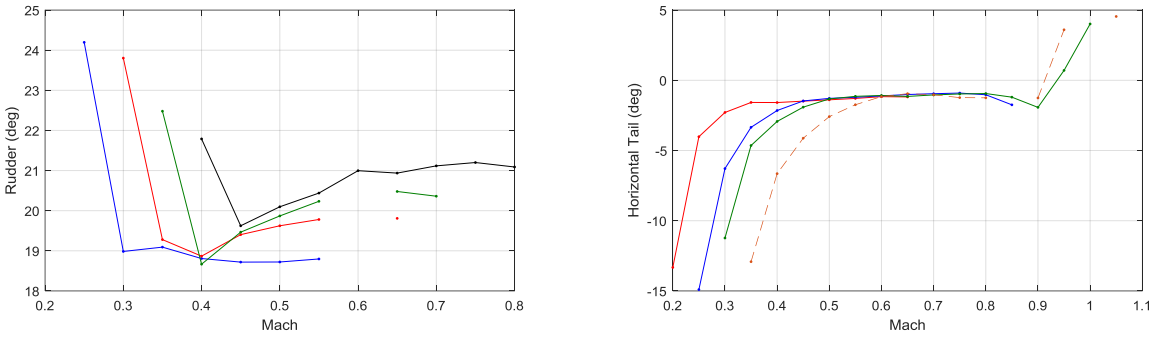

Figure 7: Variations of rudder and horizontal tail trim conditions for high sideslip angle at different altitudes

5. Analyses Conditions

For the computations between the selected interference effects, a number of analyses conditions are required to train the neural networks, linear and cubic splines and to validate these models. Wind tunnel tests and flight conditions, which are described in the previous section, are considered to determine these conditions.

ANSYS®-Fluent is used as Reynolds-averaged Navier-Stokes(RANS) flow solver to compute the flow fields around aircraft with different control surface configurations. Spalart-Allmaras turbulence model is selected with energy equation and Sutherland viscosity options. For each run, 500 and 3000 iterations are applied for the first order and the second order discretization schemes.

The interference models should be fed by the relevant data to discriminate effects of each control surfaces on the other ones. This data is called as training data. The details of the training data to represent the interference effects between rudder-horizontal tail, trailing edge flap-horizontal tail and trailing-leading edge flaps are given in Tables 1-3. In total, 1420 CFD runs are done to create training data. Due to the limitations in computational resources only one angle of attack is evaluated with multiple deflections of rudder-horizontal tail interferences.

Table 1: Rudder and horizontal tail analyses points for the interference cases

Parameter	Variable
Rudder	25, 15, 10, 5, 0
Horizontal Tail (Both)	-15,-10,-5,0,+5
Angle of Attack	0
Angle of Side Slip	-10,-5,-2,0,2,5,10
Mach	0.2, 0.4, 0.6, 0.85

DOI: 10.13009/EUCASS2019-379

Table 2: Trailing edge flap and horizontal tail analyses points for interference cases

Parameter	Variable
Trailing Edge Flap (Both)	20, 25, 30
Horizontal Tail (Both)	-15, -10, -5, 0, +5
Angle of Attack	10,15,20,25,30,35
Angle of Side Slip	0
Mach	0.2, 0.3, 0.4

Table 3: Trailing edge flap (TEF) and leading edge flap (LEF) analyses points for interference cases

Parameter	Variable
Trailing Edge Flap (Both)	20, 25, 30
Leading Edge Flap (Both)	0,10,15,20,25,30
Angle of Attack	10,15,20,25,30,35
Angle of Side Slip	0
Mach	0.2, 0.3, 0.4

To validate the interference models, a set of validation data is determined between the breakpoints of the training data. The details of the validation data are provided in Tables 4-6. Smaller deflections provided in these tables are chosen to show the insignificant interferences. It is important to note that the validation data is not included in the training data set of the neural networks, linear and cubic spline interpolations. It enables to reveal the real performance of each interference models.

Table 4: Rudder and horizontal tail analyses points for validation cases

Case	Rudder	Horizontal Tail	AOA	AOS	Mach
R-HT-1	7	+3	0	-10,-5,-2,0,2,5,10	0.80
R-HT-2	12	-8	0	-10,-5,-2,0,2,5,10	0.55
R-HT-3	20	-12	0	-10,-5,-2,0,2,5,10	0.25

Table 5: Trailing edge flap (TEF) and horizontal tail analyses points for validation cases

Case	TEF	Horizontal Tail	AOA	AOS	Mach
TEF-HT-1	22	+3	10,15,20,25,30,35	0	0.31
TEF-HT-2	24	-8	10,15,20,25,30,35	0	0.37
TEF-HT-3	27	-12	10,15,20,25,30,35	0	0.22

Table 6: Trailing edge flap(TEF) and leading edge flap (LEF) analyses points for validation cases

Case	TEF	LEF	AOA	AOS	Mach
TEF-LEF-1	27	27	10,15,20,25,30,35	0	0.21
TEF-LEF-2	24	23	10,15,20,25,30,35	0	0.28
TEF-LEF-3	22	16	10,15,20,25,30,35	0	0.35

6. Interference Modelling

In this section, the methodology of the interference effects between control surface deflections are presented. Three types of approaches including interference effects are performed in this study. These are linear interpolation method, cubic-spline interpolation method and an optimized neural network algorithm, NNGA.

For the control surface pairs of rudder-horizontal tail, drag coefficient, CD, is formulated as functions of control surface deflections to apply the interpolation methods as follows.

DOI: 10.13009/EUCASS2019-379

$$CD_{clean} = CD|_{\left(M=M_i,\ \beta=\beta_j,\ \delta_1=0,\ \delta_2=0\right)} \quad (1)$$

$$CD_{\delta_1\delta_2} = CD|_{\left(M=M_i,\ \beta=\beta_j,\ \delta_1=\delta_{1_k},\ \delta_2=\delta_{2_l}\right)} \quad (2)$$

$$\Delta CD_{\delta_1}|_{\left(M=M_i,\ \beta=\beta_j,\ \delta_1=\delta_{1_k},\ \delta_2=\delta_{2_l}\right)} = CD_{\delta_1}|_{\left(M=M_i,\ \beta=\beta_j,\ \delta_1=\delta_{1_k},\ \delta_2=0\right)} - CD_{clean} \quad (3)$$

$$\Delta CD_{\delta_2}|_{\left(M=M_i,\ \beta=\beta_j,\ \delta_1=\delta_{1_k},\ \delta_2=\delta_{2_l}\right)} = CD_{\delta_2}|_{\left(M=M_i,\ \beta=\beta_j,\ \delta_1=0,\ \delta_2=\delta_{2_l}\right)} - CD_{clean} \quad (4)$$

$$\Delta CD_{interference}|_{\left(M=M_i,\ \beta=\beta_j,\ \delta_1=\delta_{1_k},\ \delta_2=\delta_{2_l}\right)} = CD_{\delta_1\delta_2} - CD_{clean} - \Delta CD_{\delta_1} - \Delta CD_{\delta 2} \quad (5)$$

where $\boldsymbol{M_i}$ stands for each Mach number case, $\boldsymbol{\beta_j}$ stands for each angle of sideslip case, $\boldsymbol{\delta_{1_k}}$ and $\boldsymbol{\delta_{2_l}}$ stands for each control surface deflections cases considered for interference effects when angle of attack is zero as tabulated in Table 1. Clean configuration, CD_{clean}, is obtained when both control surface deflections considered herein are zero in Eq. (1) while $CD_{\delta_1\delta_2}$ is obtained for both control surfaces are deflected simultaneously in Eq. (2) for each Mach number and sideslip angle. In Eqs. (3)-(4), single control surface deflection effects are modeled as each control surface is deflected independently and the calculated CD is subtracted from CD_{clean}. Finally, interference effects between control surface deflections considered herein are calculated in Eq. (5).

Furthermore, super-impose technique, which does not include interference effects, is formulated by using Eqs. (1), (3), and (4) as

$$\Delta CD_{supimp}|_{\left(M=M_i,\ \beta=\beta_j,\ \delta_1=\delta_{1_k},\ \delta_2=\delta_{2_l}\right)} = CD_{clean} + \Delta CD_{\delta_1} + \Delta CD_{\delta 2} \quad (6)$$

where only the single control surface deflections and the clean configuration model are considered. The same formulization defined in Eqs. (1)-(6) is used for the rest of the aerodynamic coefficients (CL, CM, CR, CN, CY) when the interpolation and super-impose techniques are implemented.

Similarly, the same methodology is used for the control surface pairs of horizontal tail-trailing edge flap and trailing edge-leading edge flaps cases. For these cases, angle of attack is the variable in Eqs. (1)-(6) when sideslip angle is zero and the coefficients are calculated for the cases defined in Tables 2-3.

Governing the Eqs. (1)-(6), MATLAB®'s *interpn* command is used by selecting "*linear*" method for the linear interpolation and "*spline*" method for the cubic-spline interpolation. MATLAB®'s *interpn* command with "*linear*" method is also used to obtain super-imposed aerodynamic database.

In addition to the interpolation methods, artificial neural networks are optimized and trained by NNGA. NNGA is a genetic algorithm based neural network generation code [15]. For the rudder and horizontal tail interferences deflections, Mach number and sideslip angles are selected as input variables while the sideslip angle is switched with angle of attack for the trailing edge flap-horizontal tail and trailing edge flap-leading edge flap interferences. For each output parameter, a different neural network structure is created. The created networks are used to generate aerodynamic data for the validation cases without any additional CFD simulations.

It should be noted that the interference effect is the only difference between the model outputs and the super-impose method. The validation data set in Tables 4-6 are compared with their corresponding CFD simulations to identify the interference effects when both control surfaces are deflected simultaneously.

7. Results

In this section, comparison results of the validation data cases defined in Section 5 are presented. The comparisons are done between CFD-RANS simulations and the data obtained by interpolation methods, super-impose technique and NNGA approach defined in Section 6. Figures 8-16 show the error calculations defined as the absolute values of delta coefficients at each validation point tabulated in Tables 4-6. Delta coefficients are the variations between the CFD solution and interference models. It provides the interference effects due to the multiple control surface deflections. Super-impose technique is the sum of single deflection effects. It reveals the level of interferences. In those figures, *NNGA* represents neural network algorithm approach, *Linear* represents the linear interpolation method, *Cubic* represents the cubic-spline interpolation method and *Supimp* represents the super-impose technique.

DOI: 10.13009/EUCASS2019-379

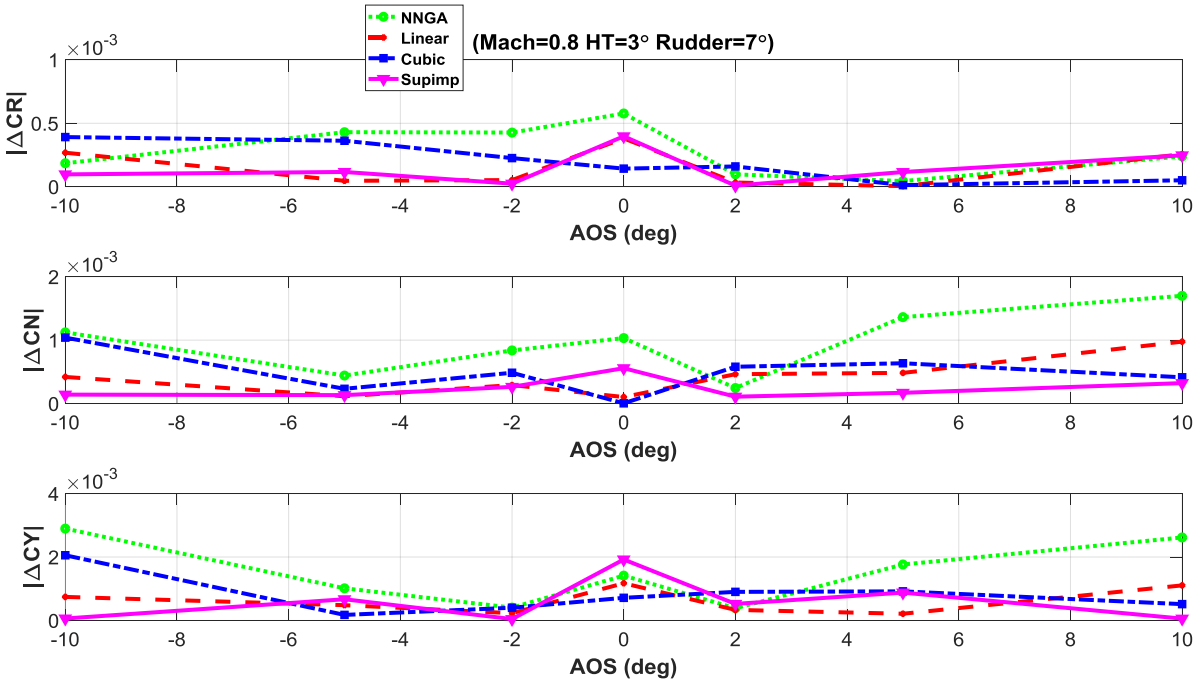

Figure 8: $\Delta CR, \Delta CN, \Delta CY$ variations with respect to angle of sideslip for the case R-HT-1

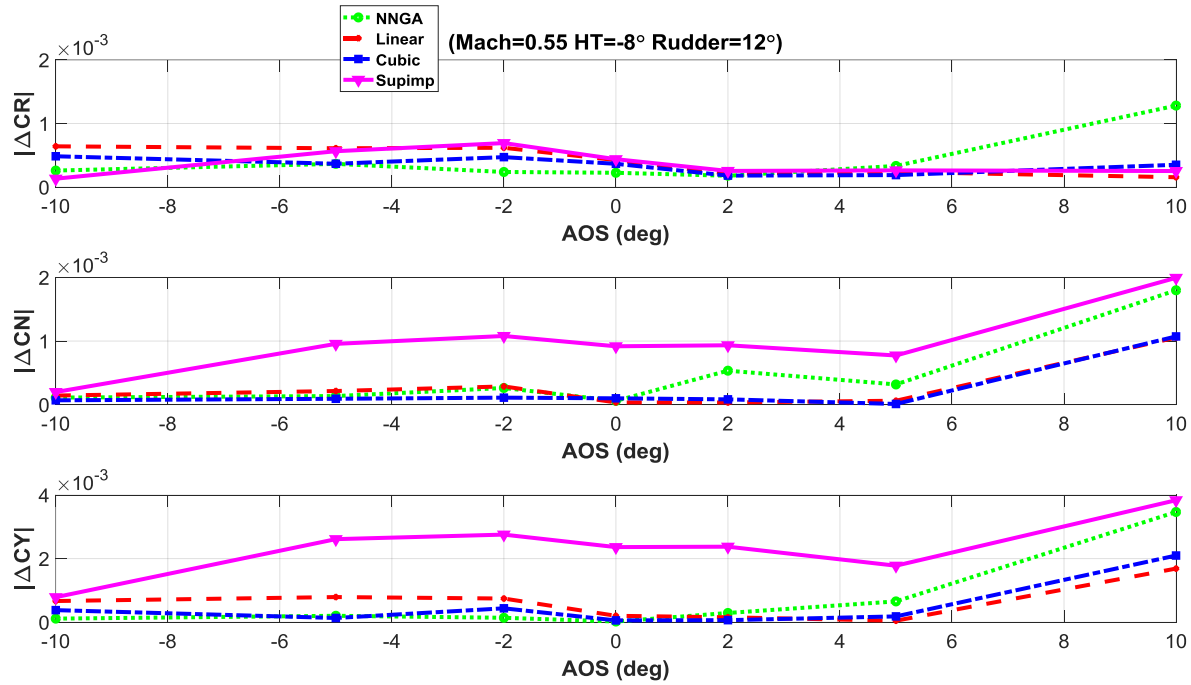

Figure 9: $\Delta CR, \Delta CN, \Delta CY$ variations with respect to angle of sideslip for the case R-HT-2

Figures 8-10 show the comparison results of $\Delta CR, \Delta CN, \Delta CY$ for the rudder-horizontal tail deflections. The super-impose technique results in the highest $\Delta CN, \Delta CY$ for higher deflections in Figs. 9-10 while NNGA gives similar performance to the linear/cubic interpolations. For positive and increasing sideslip angles in Fig. 9, ΔCN and ΔCY obtained by NNGA are higher than the linear/cubic interpolations. Nevertheless, the delta coefficients are still below the super-impose technique. On the other hand, the worst case of ΔCN and ΔCY for lower deflections (see Fig. 8) is the NNGA approach while the best case is the super-impose technique due to decreasing interference effect with lower deflections. Furthermore, ΔCR obtained by NNGA has similar results with the interpolation methods for all the test points except it is the worst with increasing sideslip angle in the positive direction in Fig. 9. Beside the comparisons,

DOI: 10.13009/EUCASS2019-379

it should be noted that calculated delta coefficients are relatively small in terms of magnitude than ΔCD and ΔCL presented in the following analyses.

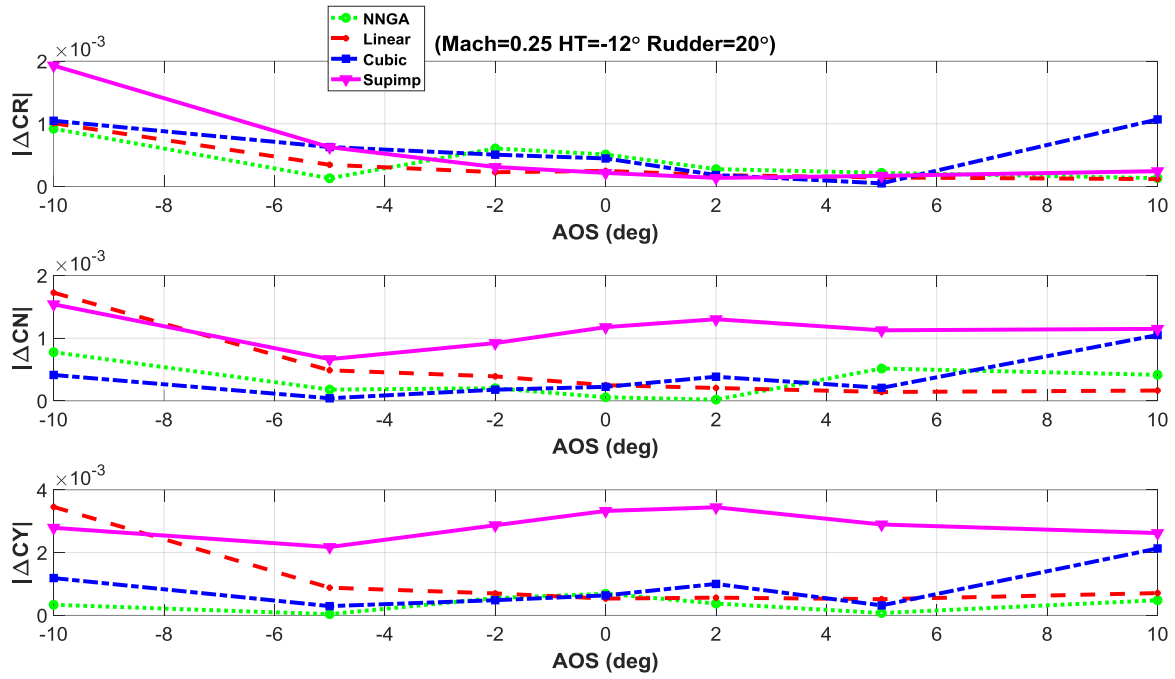

Figure 10: $\Delta CR, \Delta CN, \Delta CY$ variations with respect to angle of sideslip for the case R-HT-3

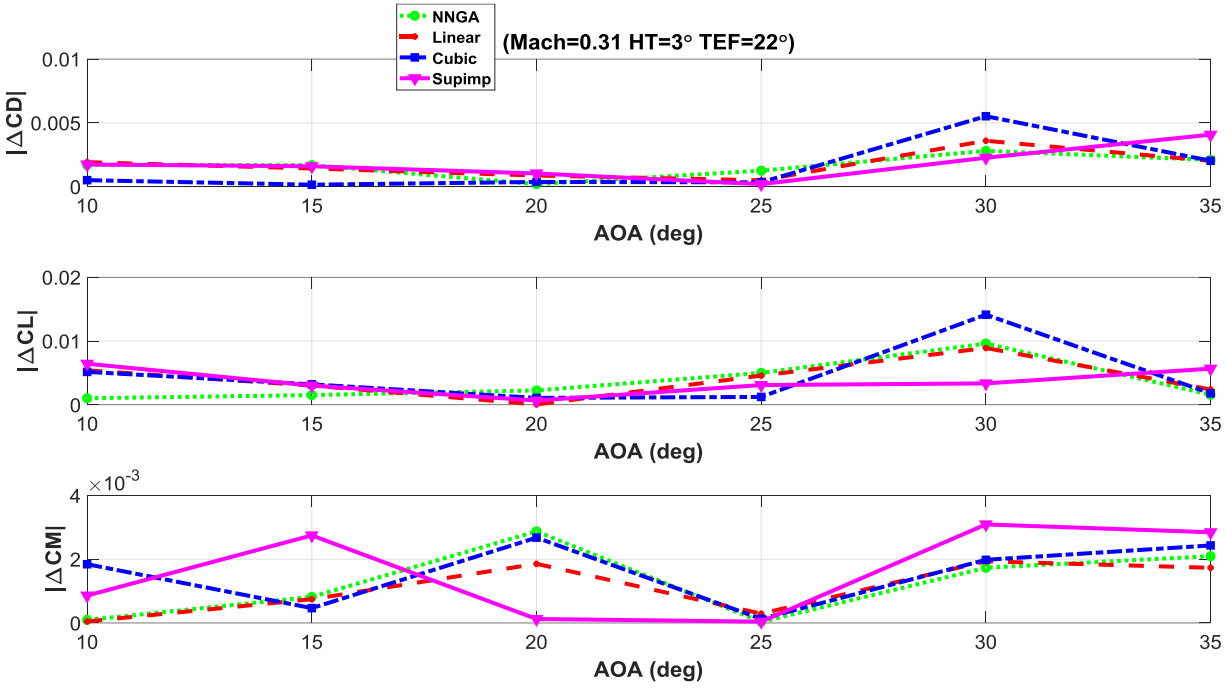

Figure 11: $\Delta CD, \Delta CL, \Delta CM$ variations with respect to angle of attack for the case TEF-HT-1

Figures 11-13 show the comparison results of $\Delta CD, \Delta CL, \Delta CM$ for horizontal tail-trailing edge flap deflections. In Fig. 11, it can be seen that NNGA is similar to the interpolation methods, especially for the cubic-spline method for all the delta coefficients. Figures 12-13 show that $\Delta CD, \Delta CL, \Delta CM$ obtained by super-impose technique is the highest up to 25 degrees of angle of attack while NNGA has a good performance as much as the interpolation methods. On the other hand, ΔCD and ΔCL obtained by linear interpolation method become worsen with increasing angle of attack beyond 25 degrees while NNGA is similar to the cubic-spline method in Fig. 12 and the super-impose technique in Fig. 13.

DOI: 10.13009/EUCASS2019-379

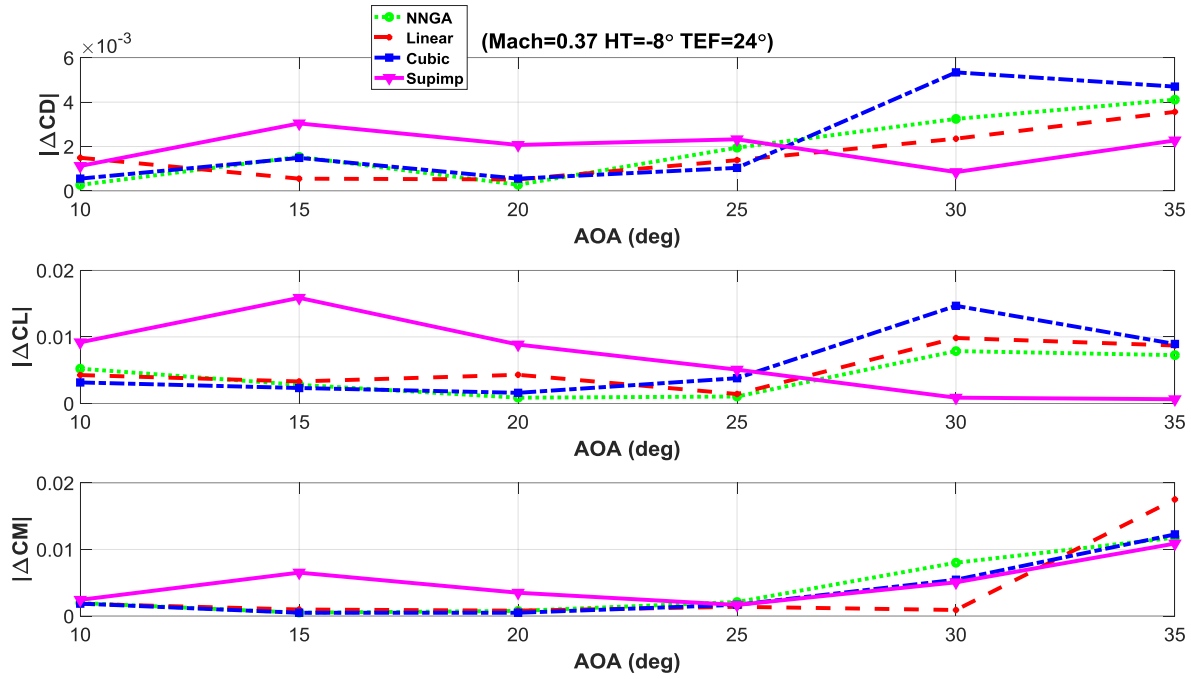

Figure 12: $\Delta CD, \Delta CL, \Delta CM$ variations with respect to angle of attack for the case TEF-HT-2

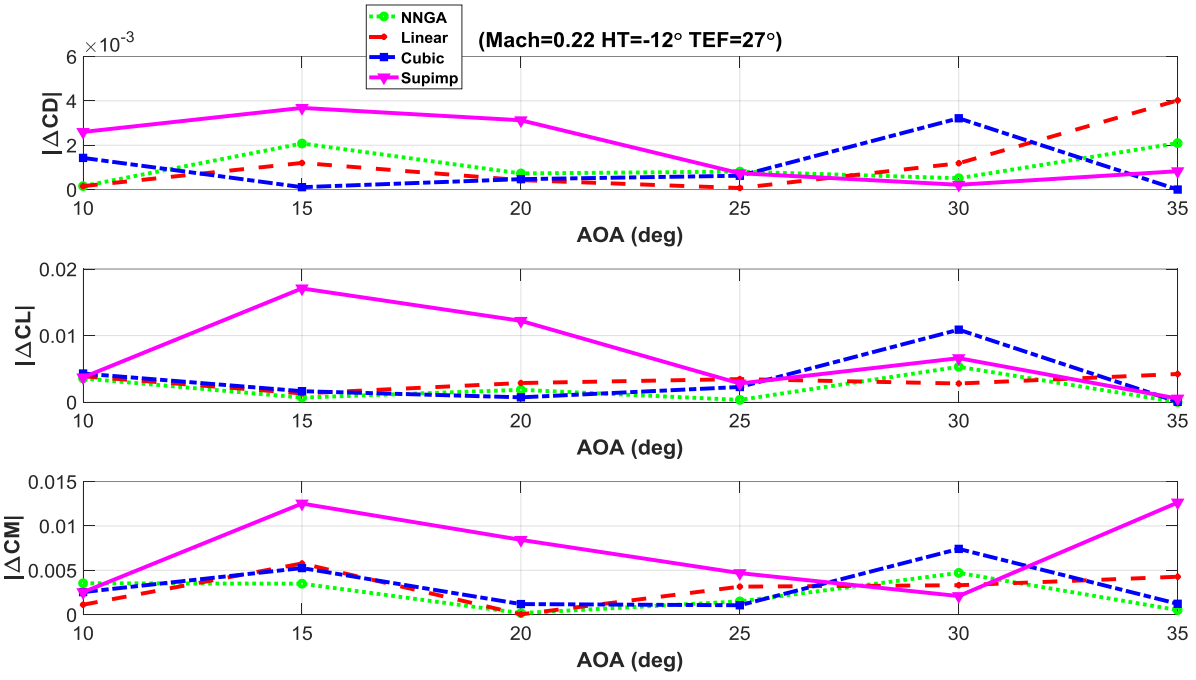

Figure 13: $\Delta CD, \Delta CL, \Delta CM$ variations with respect to angle of attack for the case TEF-HT-3

Figures 14-16 show the comparison results of $\Delta CD, \Delta CL, \Delta CM$ for trailing edge flap-leading edge flap deflections. The most important observation is that NNGA gives similar performance with the interpolation methods while super-impose technique is the worst especially for ΔCD and ΔCL for all the test cases. For the high angle of attack cases, delta coefficients obtained by super-impose technique decrease to the coefficients calculated by the rest of the methods as seen in Figs. 15-16. In Fig. 16, delta coefficients increase for higher than 30 degrees of angle of attack for the interpolation methods and the NNGA approach while the error calculated by super-impose technique decreases.

DOI: 10.13009/EUCASS2019-379

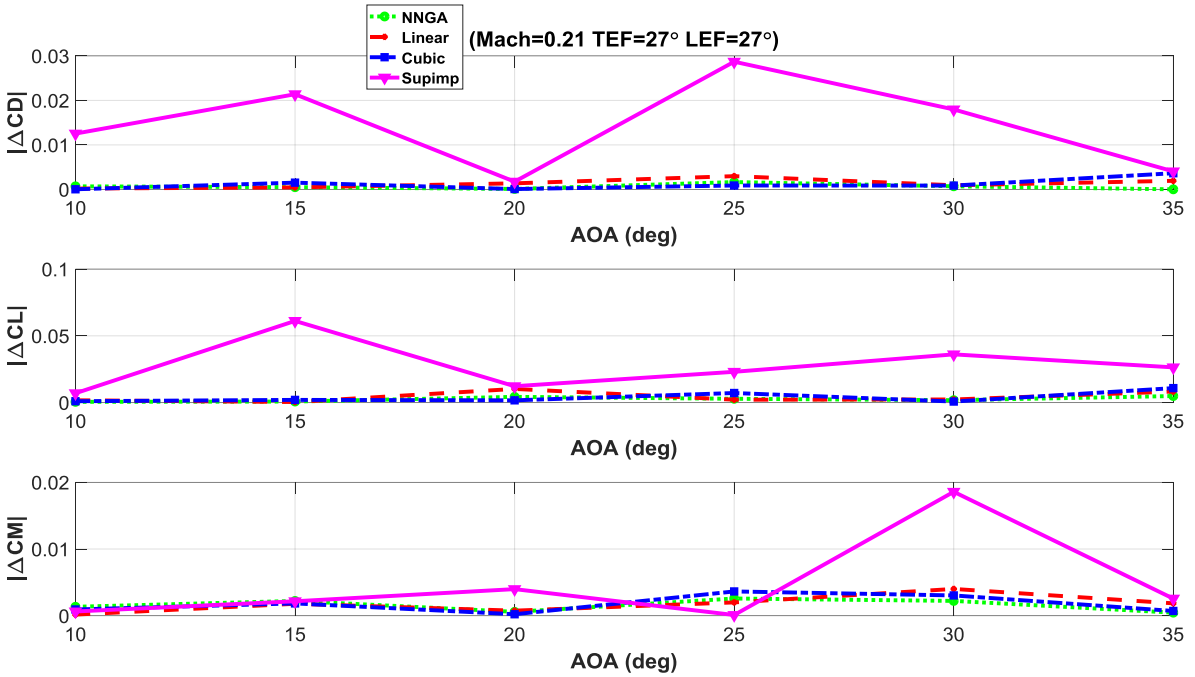

Figure 14: $\Delta CD, \Delta CL, \Delta CM$ variations with respect to angle of attack for the case TEF-LEF-1

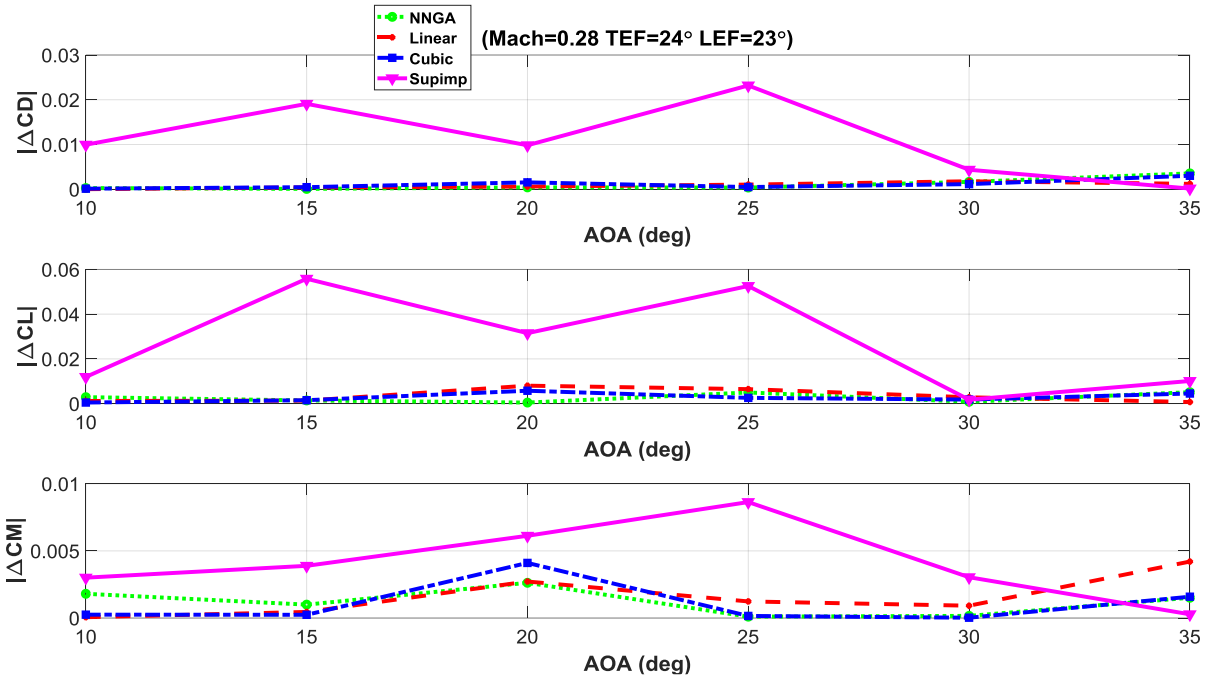

Figure 15: $\Delta CD, \Delta CL, \Delta CM$ variations with respect to angle of attack for the case TEF-LEF-2

DOI: 10.13009/EUCASS2019-379

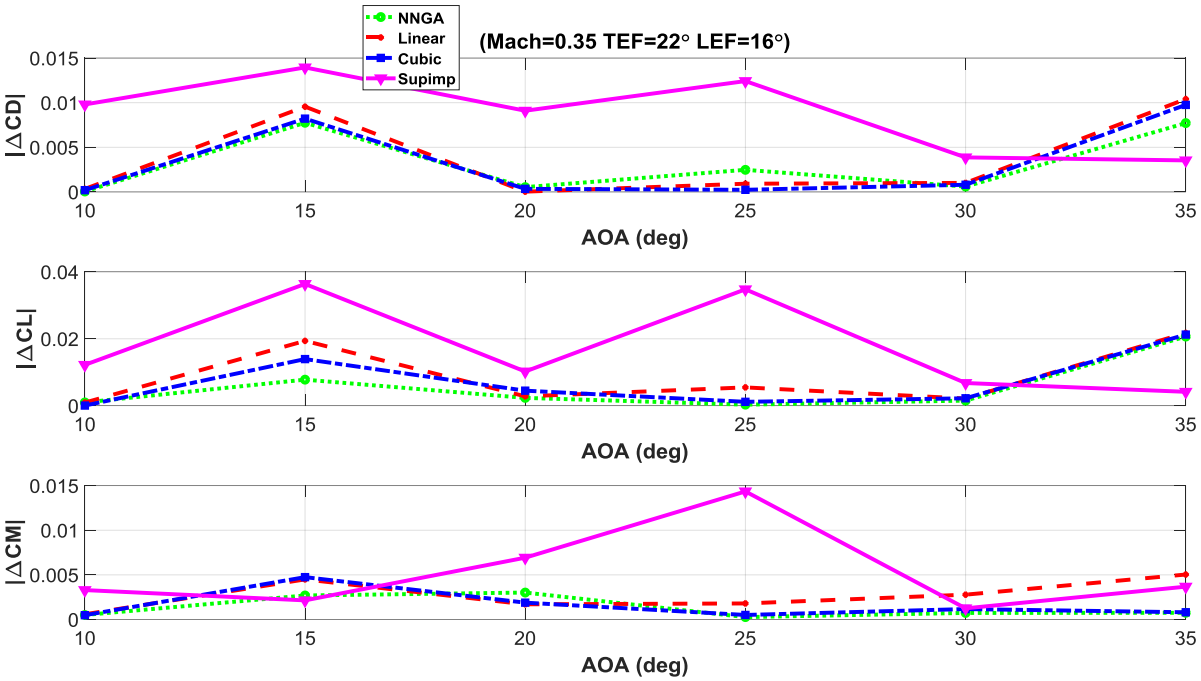

Figure 16: $\Delta CD, \Delta CL, \Delta CM$ variations with respect to angle of attack for the case TEF-LEF-3

8. Conclusion

The interference effects between rudder-horizontal tail, trailing edge flap-horizontal tail and trailing-leading edge flaps are investigated. Optimized neural networks, linear and cubic-splines are employed and their results are compared with the super-impose technique.

Different sets of analyses are determined to represent the flight conditions and control surface deflections with single and simultaneous cases. Wind tunnel tests and trim simulations are evaluated to create these sets. The sets are analyzed by CFD-RANS simulations. The outputs are involved to train neural networks or computing the coefficients of linear and cubic spline interpolations. Moreover, validation cases are created to reveal the level of interference and the performance of each model.

Interference effects between the rudder and horizontal tail are insignificant for the smaller control surface deflections. It is clearly seen that the error of super-impose method is better than the other models for these conditions. For the positive rudder deflections and negative sideslip angles, neural networks pose the smallest error for each coefficient. However, the performance of neural works decreases for the positive sideslip angles. It should be noted that the interference is computed at 0^o angle of attack. For better clarification of which model provides the best outputs, higher angle of attacks should also be investigated.

For the horizontal tail and trailing edge flap, the interference is obtained on the horizontal tail. Although the effects on the lift coefficient is slightly larger than one on the pitch moment coefficient, the highest interferences are observed on the latter. The interference is mainly due to the change in downwash angle on the horizontal tail. The maximum interference of these control surfaces is observed at the deflections of -12^o and 27^o for the horizontal tail and trailing edge flaps. This combination is very close to the takeoff conditions and can be significant effects on the takeoff rotation and takeoff distance parameters.

The maximum drag and lift changes are seen for the trailing and leading edge flap interferences. Since the takeoff and landing conditions strongly involves trailing and leading edge flap deflections, the interferences between them should be modelled in the plant model. Moreover, if the aircraft has flaperon instead of the flaps these effects should be investigated for the higher velocity regimes.

DOI: 10.13009/EUCASS2019-379

References

[1] D. Linse and R. Stengel , "Identification of Aerodynamic Coefficients Using Computational Neural Networks," *Journal of Guidance, Control and Dynamics,* vol. 16, no. 6, 1993.

[2] N. Frink, P. Murphy, H. Atkins, S. Viken, J. Petrilli, A. Gopalarathnam and R. Paul, "Computational Aerodynamic Modeling Tool for Aircraft Loss of Control," *Journal of Guidance, Control and Dynamics,* vol. 40, no. 04, 2017.

[3] O. Al-Shamma, R. Ali and H. Hasan, "Employing control surface model in preliminary aircraft design software," *International Journal of Engineering and Technology,* vol. 7, pp. 135-140, 2018.

[4] J. E. Steck and K. Rokhsaz, "Some applications of artificial neural networks in modeling of nonlinear aerodynamics and flight dynamics," in *35th Aerospace Sciences Meeting and Exhibit*, Reno, NV, 1997.

[5] J. Scharl and D. Mavris, "Building Parametric and Probabilistic Dynamic Vehicle Models Using Neural Networks," in *AIAA Modeling and Simulation Technologies Conference and Exhibit*, Montreal, Canada, 2001.

[6] S. Kottapalli, "Neural-network-based modeling of rotorcraft vibration for real-time applications," in *AIAA Modeling and Simulation Technologies Conference and Exhibit*, Denver, CO, 2000.

[7] R. Mori, S. Suzuki, Y. Sakamoto and H. Takahara, "Analysis of Visual Cues During Landing Phase by Using Neural Network Modeling," *Journal of Aircraft,* vol. 44, no. 6, pp. 2006-2011, 2007.

[8] A. A. Trani, F. C. Wing-Ho, G. Schilling, H. Baik and A. Seshadri, "A Neural Network Model to Estimate Aircraft Fuel Consumption," in *AIAA 4th Aviation Technology, Integration and Operations (ATIO) Forum*, Chicago, IL, 2004.

[9] G. Richey, "Aerodynamics of Combat Aircraft Controls and of Ground Effects," AGARD Advisory Report 271, Ohio, 1991.

[10] D. Levin, "A Vortex Lattice Method for Calculating Lifting-Surface Interference," in *AIAA Aircraft Systems and Technology Conference*, Dayton, Ohio, 1981.

[11] J. Elzebda, D. Mook and A. Nayfeh, "Numerical Simulation of Steady and Unsteady, Vorticity-Dominated Aerodynamic Interference," *Journal of Aircraft,* vol. 31, no. 05, 1994.

[12] F. Moore and R. McInville, "A new semiempirical model for wing-tail interference," in *AIAA Atmospheric Flight Mechanics Conference*, San Diego,CA , 1996.

[13] R. Kulfan, "Application of Hypersonic Favorable Aerodynamic Interference Concepts to Supersonic Aircraft," in *AIAA Aircraft Systems and Technology Conference*, Los Angeles, California, 1978.

[14] D. Landman, J. Simpson, D. Vicroy and P. Parker, "Response Surface Methods for Efficient Complex Aircraft Configuration Aerodynamic Characterization," *Journal of Aircraft,* vol. 44, no. 04, 2007.

[15] F. Gomec and M. Canibek, "Aerodynamic Database Improvement of Aircraft based on Neural Networks and Genetic Algorithms," in *7TH European conference for Aeronautics and Space Sciences (EUCASS),* Milano, 2017.